GPU Accelerated Numerical Simulation of Local Scours Near Hydraulic Structures

Vladimir Prokofev

ABSTRACT

A module of sediments transport allowing to simulate the dynamics of local bed scours in proximity to hydraulic structures has been integrated into the three-dimensional non- hydrostatic multilayer open flow model. The sediment transport calculation is performed based on the formulas that apply the value of bed-shear stress. The slope slide in the scour hole and the alteration of the critical shear stress depending on the local bed inclination and flow speed direction are taken into account. This numerical model has been implemented completely by means of a GPU which allows to perform complicated 3D calculations within a reasonable time period. The results of testing performed based on the publicly available experimental data are given: comparison of the dynamics of bed transformation behind the apron as influenced by jet current is performed; development of local scours in proximity to the vertical circular pile is validated based on the results of large-scale experiments.

Keywords: local scours; GPU calculations; non-hydrostatic; openCL; sediment transport; three-dimensional multilayer model.

Classification: DDC Code: 621.51 LCC Code: TJ840'

Language: English

London Journals Press

LJP Copyright ID: 392923
Print ISSN: 2631-8474
Online ISSN: 2631-8482

London Journal of Engineering Research

Volume 22 | Issue 8 | Compilation 1.0

GPU Accelerated Numerical Simulation of Local Scours Near Hydraulic Structures

Vladimir Prokofev

ABSTRACT

A module of sediments transport allowing to simulate the dynamics of local bed scours in proximity to hydraulic structures has been integrated into the three-dimensional non- hydrostatic multilayer open flow model. The sediment transport calculation is performed based on the formulas that apply the value of bed-shear stress. The slope slide in the scour hole and the alteration of the critical shear stress depending on the local bed inclination and flow speed direction are taken into account. This numerical model has been implemented completely by means of a GPU which allows to perform complicated 3D calculations within a reasonable time period. The results of testing performed based on the publicly available experimental data are given: comparison of the dynamics of bed transformation behind the apron as influenced by jet current is performed; development of local scours in proximity to the vertical circular pile is validated based on the results of large-scale experiments.

Keywords: local scours; GPU calculations; non-hydrostatic; openCL; sediment transport; three-dimensional multilayer model.

Author: Post-doctoral Researcher. *RusHYDRO, Hydraulic department of Vedeneev VNIIG, Russia.*

I. INTRODUCTION

Simulation of sediment transport and development of bed scours in proximity to hydraulic structures (HS) based on both physical and numerical models pertains to one of the most complicated and controversial fields of open flow hydraulics. Flow hydrodynamics – flow field, distribution of hydrodynamic pressure values and turbulence parameters in a flow – are simulated quite successfully by means of many modern numerical models including three-dimensional ones. The only difficulty that still remains is a significant time required to perform calculations for 3D tasks related to hydrodynamics which can equal a period of several days or even dozens of days. Using graphical processing units (GPU) allows to circumvent this restriction – Prokofyev (2017).

Numerical simulation of suspended and bedload sediments transport represents a more complicated task. There are dozens of formulas and models allowing to forecast bed deformations. However, calculations performed using such formulas and models are at the same time characterized by significant scatter of forecasting results, by one order or even more, especially in cases when not only the final depth of the scour holes or the height of the sediment deposits, but also simulation of their development in time are at issue. The criterion for estimation of the practical applicability of a particular model in HS engineering practice is validation of this model based on experimental data – field data or laboratory data.

There are cases when a numerical model is calibrated prior to its application for bed scour calculations with regard to a particular HS, which is quite logical. Still, in most cases initial data are not sufficient or reliable enough to perform such calibration. Moreover, even when the data set required for calibration is available, it is preferable that the model which has been tested based on experimental material be used as a baseline model for bed scours. It is also desirable that the set of free parameters of the model to be calibrated require no adjustment for each individual experiment *and be universal.* The present research is dedicated

to development of such baseline model and its testing based on experimental data obtained by third-party authors.

II. EDDY VISCOSITY SIMULATION

RANS numerical models for open flow hydrodynamics, both planimetric and three-dimensional, are well known. 2.5D description of a hydrodynamic model applying the so-called σ-coordinates for vertical discretization has been written by Audusse et al. (2011); the designation 2.5D corresponds to the use of a multilayer model in approximation of hydrostatic distribution of pressure over the flow depth. But in their turn, more complicated 3D multilayer open flow models consider the difference between the distribution of pressure over the flow depth and the hydrostatic one (Stelling & Zijlema, 2008; Ma et al., 2012; Prokofev, 2018), which requires that the Poisson equation be solved at each time step with the purpose of non-hydrostatic pressure correction. It was a full 3D model of open flow hydrodynamics that was taken as a basis for the sediments transport and bed scours model, and due to its stricter requirements to computational resources, it was fully implemented for the performance of calculations in a graphical processing unit – GPU (Prokofyev, 2017). We are not going to specify its description again here, f.e. by giving mass and momentum exchange equations in case of multilayer vertical discretization, but we are going to focus only on the modifications introduced to the model and its peculiarities that are important when bed scours simulation is performed. We shall specify that the algorithm is based on an explicit second order time accuracy prediction-correction scheme. During each time step, the simplest iteration method that is quickly convergent and efficiently implemented for GPU is used for solving the Poisson equation with the purpose of non-hydrostatic pressure correction (Prokofev, 2018). The model ensures conservation (exact fulfillment of the conservation laws for a discrete form) of exchange of mass, momentum and other substances.

First of all, the model shall be supplemented with the eddy viscosity calculation module based on the widely used *k*-ε turbulence model. Eddy viscosity is written as an (Belov & Kudriavtsev, 1987; Lin & Liu, 1998)

$$\nu_t = C_\mu \cdot k^2 / \varepsilon \ ,$$

equation for exchange of turbulence kinetic energy k (TKE) and its dissipation rate ε :

$$\frac{\partial k}{\partial t} + \nabla \bullet \left(\boldsymbol{u} \cdot k \right) = \nabla \bullet \left[\left(\nu + \frac{\nu_t}{\sigma_k} \right) \nabla k \right] + Prod - \varepsilon \ , \tag{1}$$

$$\frac{\partial \varepsilon}{\partial t} + \nabla \bullet \left(\boldsymbol{u} \cdot \varepsilon \right) = \nabla \bullet \left[\left(\nu + \frac{\nu_t}{\sigma_\varepsilon} \right) \nabla \varepsilon \right] + C_{1\varepsilon} \frac{\varepsilon}{k} Prod - C_{2\varepsilon} \frac{\varepsilon^2}{k} \ . \tag{2}$$

In case of equations (1) and (2): t – time, ν – liquid kinematic viscosity, while the turbulent production rate $Prod$ for an incompressible liquid is defined using the magnitude of the strain-rate tensor S:

$$Prod = \nu_t S^2; \quad S^2 = \left(\frac{\partial u_i}{\partial x_j} + \frac{\partial u_j}{\partial x_i} \right) \frac{\partial u_i}{\partial x_j} \ , \tag{3}$$

where x_i – coordinate, u_i – current velocity vector components $\boldsymbol{u}$, summation is performed over the $i = 1,2,3$ repeated index. Standard set of constants for the *k*-ε turbulence model: $C_\mu = 0.09;\ \sigma_k = 1.0;\ \sigma_\varepsilon = 1.3;\ \ C_{1\varepsilon} = 1.44;\ C_{2\varepsilon} = 1.92$. Wu et al. (2004) compare other

London Journal of Engineering Research

types of the *k*-ε turbulence model, f.e. the Non-equilibrium *k*-ε model and RNG turbulence model which differ primarily from the standard one in the set of these 4 constants. In particular, the following values are assumed for the RNG model: $C_\mu = 0.085$; $\sigma_k = 0.7179$; $\sigma_\varepsilon = 0.7179$; $C_{2\varepsilon} = 1.68$, and the constant $C_{1\varepsilon}$ becomes the parameter depending from the value *S* in this particular point (Wu et al., 2004; WAQUA/TRIWAQ, n.d.):

$$C_{1\varepsilon} = 1.42 - \frac{\eta\left(1-\eta/4.38\right)}{1+0.015\cdot\eta^3}, \quad \eta = \frac{k\cdot S}{\varepsilon}.$$

The wall functions technique is widely used for setting boundary conditions for the turbulence parameters *k* and ε at the bed (Belov & Kudriavtsev, 1987; Wu et al., 2004; Kuzmin et al., 2007). In our research, we apply multilayer flow depth discretization (Audusse et al., 2011; Prokofev, 2018), so the use of the above-mentioned method comes down to special recording of the (1) and (2) discrete equation analogs in the lower (near-bottom) layer and TKE production rate (3). The TKE dissipation rate exchange equation ε (2) in the lower computation layer is not solved. Instead of this, ε in the middle of the layer is calculated directly using the value *k* in the middle of the relevant layer that has already been defined by applying the exchange equation (1) (Belov & Kudriavtsev, 1987; Wu et al., 2004):

$$\varepsilon = C_\mu^{3/4}\cdot k^{3/2} \Big/ \left(\mathrm{K}\cdot z^+\right), \tag{4}$$

where $\mathrm{K} = 0.41$ – Von Karman constant, z^+ – distance from the reference computation node to the bed. In case of near-bed computation layer, it is considered that the convective and diffusion exchange *k* through the lower surface of the layer is absent. The strain-rate tensor *S* components (3) defined trough derivatives of bed-wise tangent velocity components cannot be precisely calculated in case of the near-bed layer using the finite differences: the current velocity increases too rapidly as moving up from the bed in compliance with the logarithmic law. That is why the wall-functions technique (Belov & Kudriavtsev, 1987) is used here as well, so that the derivatives that are out of the viscous sublayer are calculated based on the logarithmic near-bed velocity profile (Kim et al., 2017; Török et al., 2017]:

$$z = z^+ : \quad \frac{\partial \boldsymbol{V}}{\partial N} = \frac{\boldsymbol{V}}{z^+\ln\left(z^+/z_0\right)}, \tag{5}$$

where $\boldsymbol{V}$ – current velocity vector in the mesh node that is the closest to the bed, situated at the distance of $z^+ > z_0$ from the bed, *N* – hereinafter represents the boundary normal, z_0 – bed roughness parameter. The last example is in some cases expressed as $k_s/30$, where k_s is the Nikuradse's roughness parameter (Kim et al., 2017). In case of condition (5) the velocity along the bed is taken as the rate $\boldsymbol{V}$, so the local slope angle is considered. The bed-shear stress required to solve the system of hydrodynamic equations may be expressed through the value of TKE or the flow speed in the near-bed computation node in case the *k*-ε model is applied (the one belonging to the previous time step is taken) (Wu et al., 2004; Belov & Kudriavtsev, 1987, p.133):

$$\boldsymbol{\tau} = \boldsymbol{V}\cdot\rho\cdot\mathrm{K}\cdot C_\mu^{1/4}\cdot\sqrt{k} \Big/ \ln\left(z^+/z_0\right), \tag{6}$$

where ρ – water density. Török et al. (2017) use $|\boldsymbol{\tau}| = \rho\cdot k\sqrt{C_\mu}$ instead of (6), but within the context of the present research such recording format is less convenient: it does not define the direction of $\boldsymbol{\tau}$ (Belov & Kudriavtsev, 1987).

London Journal of Engineering Research

In case of free surface, soft boundary conditions are commonly used for the turbulence parameters k and ε (Lin & Liu, 1998) – absence of their convective and diffusion exchange through the upper boundary of the surface computation layer:

$$\partial k / \partial N = \partial \varepsilon / \partial N = 0 \quad . \tag{7}$$

The specific distribution of k, ε, ν_t, V over the flow depth obtained through experiments under conditions of a uniform steady current in an open channel can be found in the research paper by Violeau & Issa (2007). These values show that the condition (7) which is widely used on the free surface referring to k is characterized by limited applicability; Török et al. (2017) set $k = 0$ on the surface. The turbulent production rate *Prod* (3) in the upper layer was calculated using the standard procedure: wall functions were not involved. Setting soft boundary condition (7) for ε on a free surface also represents a disputable issue: such a condition corresponds to the predominance of turbulence with the vertical axis of eddy currents. If the eddy exchange based on the flow depth is the main factor and this exchange is defined by eddy currents with the horizontal axis, it is more logical to set condition (4) for ε on a free surface and consider z^+ to be the distance from the computation node in the middle of the upper layer to the surface. The horizontal and vertical scales of turbulence can be significantly different (Voltsinger et al., 1989), in other words, eddy exchange is anisotropic and that is why in some cases 2 models are used to describe it: separately for horizontal and vertical directions (Rodriguez-Cuevas et al., 2014; WAQUA/TRIWAQ, n.d.).

In case of the impermeable boundaries of the computation domain (vertical walls), the boundary conditions set for the k и ε turbulence parameters were set to be same as those for the bed, however, additional TKE production rate was not calculated using the (5) formula: the walls were assumed to be smooth. In case of open vertical boundaries of the computation domain, the soft boundary conditions (7) were set in cases of outflow. In case of inflow through the boundary, a profile of k and ε that was close to the equilibrium one was set (Kuzmin et al., 2007):

$$k = \frac{U_*^2}{\sqrt{C_\mu}} \quad , \quad \varepsilon = \frac{C_\mu^{3/4} \cdot k^{3/2}}{\mathrm{K} \cdot h(1-\sigma)\sigma} \quad , \tag{8}$$

where h – depth in area of the boundary with inflow, $U_* = \sqrt{\tau / \rho}$ – bed-shear velocity, σ – dimensionless distance from the middle of the relevant computation layer to the bed (normalized for h: at the bed $\sigma = 0$, on free surface $\sigma = 1$). Based on test calculations, a soft boundary condition may also be set for k in case of sub-critical inflow: $\partial k / \partial N = 0$, and ε is to be determined based on (8) through k (TKE) in the near-boundary computation node, taking the relevant value from the previous time step.

The discrete form of the exchange equation for the k and ε turbulence parameters is written applying a conservative format, the same as in case of exchange equations for the momentum components or other substance in numerical multilayer open flow models (Audusse et al., 2011). In case of horizontal coordinates, the finite volume method (FV) is used while in case of vertical coordinates adaptive mesh is used (σ-coordinates), Prokofev (2018). In this case, the convective and diffusion exchange of the turbulence parameters between the computation layers is taken into account. In order to increase the scheme accuracy to the second order of magnitude when recording convective fluxes through the FV cell faces and between the layers, the TVD reconstruction is used (Kulikovskii et al., 2001).

In case of approximation of depth, bed levels and horizontal components of the current rate in the FV cell faces, the UNO scheme was used (Kulikovskii et al., 2001, p.115) as it ensures the highest accuracy of fluxes approximation and is better for description of the eddy

current structures which are formed for example when flowing around the circular cylinder. As opposed to less complicated reconstruction schemes (used for k, ε and convective exchange between the computation nodes), a 5 point skeleton instead of a 3 point one is generated; the points are located along the computation mesh line that passes through the FV cell face. We are going to express the values in the above-mentioned points that were already obtained during the previous time step using the following $Z_m;\ m=1,2,3,4,5$: in order to perform reconstruction, the derivative $\partial Z/\partial m$ in Z_3 point shall be determined. In case of standard 3 point schemes of TVD reconstruction, this derivative is determined by means of increment addition in order to ensure stability

$$dZ_3 = \text{Limiter}\left(Z_4 - Z_3,\ Z_3 - Z_2\right).$$

In this case, the function Limiter (A,B) that depends on the two parameters represents a limiter, f.e. the simplest MinMod. The above-mentioned limiter and other well-known limiters are specified in the book Kulikovskii et al. (2001). In case of the 5 point UNO scheme, the three additional parameters are determined first

$$D_m = \left(Z_{m-1} + Z_{m+1}\right)/2 - Z_m; \qquad m = 2,3,4 \quad ,$$

followed by the necessary increment value in the point Z_3

$$dZ_3 = \text{Limiter}\left[Z_3 - Z_2 + \text{Limiter}\left(D_2, D_3\right),\ Z_4 - Z_3 - \text{Limiter}\left(D_3, D_4\right)\right].$$

As the Limiter (A,B) for practical calculations, the Van Leer limiter can be taken, however, the same approximation accuracy with lower pulsations in the field of a moving bore (test task) is provided by the next limiter. In case of different values of the parameters A and B, it normally equals zero but in other cases the

$$\text{Limiter}\left(A,B\right) = 0.5 \times \begin{cases} \min\left(A, \alpha B\right) + \min\left(B, \alpha A\right)\ , & A > 0 \\ \max\left(A, \alpha B\right) + \max\left(B, \alpha A\right)\ , & A < 0 \end{cases}.$$

Parameter α may be represented by any value from the range [1..2]; we used the value $\alpha = \sqrt{2}$. This limiter shall not be confused with the well known SuperBee limiter: even with $\alpha = 2$ they are not congruent. In proximity to the boundaries of the computation domain, the 5 point reconstruction scheme has to be transformed into a 3 point one become a 5 point skeleton cannot be constructed.

The multilayer open flow model written using adaptive σ-coordinates allows for using the vertical mesh with condensation near the free surface (which may be useful when solving wave problems) and/or near the bed. The computation mesh condensation near the bed allows to save computational resources when solving tasks related to transport of sediments and bed scours. We applied mesh condensation near the bed based on hyperbolic functions:

$$\sigma\left(l\right) = \sinh\left(\beta l / L\right)/\sinh\left(\beta\right)\ , \qquad 0 \le l \le L\ , \tag{9}$$

$$\beta = \text{arccosh}\left(E\right), \qquad E = \Delta\sigma^{\max}/\Delta\sigma^{\min}\ .$$

Here: L – number of computation layers, the layers are given numbers from 0 (near the bed) to L-1; the parameter E sets the required mesh condensation, namely a relation between the thickness of the layer near the free surface versus the thickness of the near-bed layer. The dimensionless coordinate related, for example, to the medium level of the 3rd layer is located as per (9), the same as $\sigma\left(3.5\right)$, and the same coordinate of the lower boundary is $\sigma\left(3.0\right)$.

London Journal of Engineering Research

III. TRANSPORT OF SUSPENDED AND BEDLOAD SEDIMENTS

In addition to the *k*-ε module of the turbulence model, a computation module for sediment transport and bed scours has been added to the multilayer open flow model. Let's focus on some of its peculiarities that are important when simulating local bed scours in the context of the text tasks given below:

- procedure for re-calculation of the suspended load transport into erosion rate: volume of soil that is converted into a suspended state near the bed per unit time;
- consideration of the local bed slope during calculation of a critical shear stresses;
- simulation of slides of soil slopes formed in the context of re-formation of the bed in cases when their angle reaches the limit value.

The particle fall velocity is calculated using the Soulsby's formula (1997)

$$w = \frac{\nu}{d}\left(\sqrt{10.36^2 + 1.094 \cdot D_*^3} - 10.36\right), \tag{10}$$

where d – diameter of sediment particles, $D_* = d\left(\varphi_\rho \cdot g / \nu^2\right)^{1/3}$ – dimensionless diameter of particles, $\varphi_\rho = (\rho_s - \rho)/\rho$, ρ_s – sediment skeleton density, g – gravity acceleration, ν – kinematic water viscosity calculated using the Poiseuille's formula at the temperature T set in degrees C

$$\nu = 1.78 \times 10^{-6} \Big/ \left(1 + 0.0337 \cdot T + 0.000221\sqrt{T}\right), \ (\mathrm{m^2\,s^{-1}}). \tag{11}$$

In order to calculate the suspended load transport rate the Van Rijn's formula (2012), for example, can be used

$$q_s = 0.008 \cdot \overline{V} \cdot d \cdot M_e^{2.4} \cdot D_*^{-0.6}, \tag{12}$$

where the dimensionless mobility parameter of sediment particles with the depth-averaged flow speed is $\overline{V}$

$$M_e = \left(\overline{V} - V_{CR}\right) / \sqrt{\varphi_\rho \cdot g \cdot d}.$$

The dimensionless diameter D_* and the particle fall velocity w (10) are significantly dependent on the water kinematic viscosity (11) and consequently on its temperature. Depth averaged critical velocity corresponding to the initiation of the particles motion for Van Rijn's formula (12)

$$V_{CR} = 5.75 \cdot \mathrm{Lg}_{10}\left(2h/d\right)\sqrt{\theta_{CR} \cdot \varphi_\rho \cdot g \cdot d},$$

where the dimensionless critical Shields's parameter is

$$\theta_{CR} = 0.3/\left(1 + 1.2\,D_*\right) + 0.055\left[1 - \exp\left(-0.02 D_*\right)\right]. \tag{13}$$

Apart from Van Rijn's formula (12), there are at least several dozens of other formulas allowing to estimate the suspended load particles transport, generated based on both field data and laboratory measurements carried out in hydraulic flumes just like in (12). However, in case of such an averaged format the connection between the depth-averaged suspended sediment transport load q_s and the depth-average flow speed $\overline{V}$ (or even the bed-shear stress measured with regard to such a speed) cannot be used directly in a numerical 3D convective-diffusion model of suspended particles exchange. In case of such a model, it is necessary to connect, for example, the local value of bed-shear stress τ with the lifted particle's flux from the packed bed in the near-bed layer. For this purpose, it will be required to adapt formula (12) or any other similar one to re-calculate the suspended load transport of the flow into its *erosion rate.* Taking into account that Van Rijn's (2012) experiments were carried out under a

London Journal of Engineering Research

uniform and steady flow condition, we can take the profile of the eddy viscosity distribution over the flow depth using Montgomery's parabolic formula (Voltsinger et al., 1989):

$$\nu_t(\sigma) = \mathrm{K} \cdot h \cdot U_* (1-\sigma)\sigma \ . \tag{14}$$

The steady state distribution of volumetric concentrations of suspended particles $c(\sigma)$ over the depth in a uniform flow shall be compliant with the stationary one-dimensional convective and diffusion vertical exchange equation (Van Rijn, 2012):

$$\frac{\nu_t(\sigma)}{h}\frac{dc}{d\sigma} = -w \cdot c \ . \tag{15}$$

If we put the turbulence viscosity profile (14) into this equation, once the variables and integration values are substituted, we can find an analytical solution (15) – Rouse's *equilibrium* concentrations profile (Van Rijn, 2012; Delft3D-FLOW, 2005; Amoudry, 2008)

$$c(\sigma) = c_0 \left[\frac{\sigma_0(1-\sigma)}{\sigma(1-\sigma_0)}\right]^{\frac{w}{\mathrm{K}U_*}} , \tag{16}$$

where c_0 – concentration at a dimensionless distance from the bed σ_0, in our case this may be a medium level in the lower computation layer. A *non-equilibrium* profile is used in Delft3D-FLOW (2005) as well when the power indicator (16) is defined in the course of calculations related to the vertical concentrations gradient during the previous time step: we do not need it *now*. The concentration profile (16) is characterized by singularity at $\sigma \to 0$, that is why in order to evaluate the relation between the suspended load transport q_s and the near-bed concentration c_0, Rouse's profile, when the w and U_* values were known, was integrated within the range $[\sigma_{\min} \ldots 1]$:

$$q_s = c_0 \cdot h \int_{\sigma_{\min}}^{1} V(\sigma)\left[\frac{\sigma_0(1-\sigma)}{\sigma(1-\sigma_0)}\right]^{\frac{w}{\mathrm{K}U_*}} d\sigma \, . \tag{17}$$

Where $V(\sigma)$ – velocity profile. Logarithmic profile, for example. With the σ_0, $\sigma_{\min}$ parameters set and the bed-shear velocity U_* that also defines the $V(\sigma)$, numerical integration (17) can be carried out using the simplest quadrature formulas. It gives linear connection $c_0 = r \cdot q_s$. The $\sigma_{\min} \le \sigma_0$ parameter was set to be equal to 0.005, and in case of additional test calculations for suspended sediments (*test 2* below) it varied for evaluating the influence of $\sigma_{\min}$ on the results: it was not found. This is explained by the fact that in the area near the bed $V(\sigma) \to 0$, that is why singularity does not show itself in case of expression under integral sign (17); standard profiles $V(\sigma), c(\sigma)$ and their derivatives are specified in Van Rijn (2012).

A similar but not identical procedure for defining concentrations for near-bed computation layers with the use of Rouse profile (16) can be found in the description Delft3D-FLOW (2005), and in that case the concentration at the low level σ_0 is therein called a "reference" one (see also Van Rijn, 2012; Amoudry, 2008). Thus in case of an experiment with a *uniform current*, we can move from suspended load transport rate q_s calculated using (12) or any other empirical formula into the reference concentration c_0 near the bed, for example in the middle of the near-bed computation layer. When the empirical

London Journal of Engineering Research

formula for q_s is generated based on depth-averaged flow speeds, as in our case (12), but not based on bed-shear stresses τ, first of all re-calculation is to be performed $\overline{V} = f(\tau)$. It is clear that if during such a laboratory experiment the flow transports a quantity of suspended sediments complying with its transport rate, dynamic equilibrium of sediment particles elevation and sedimentation is observed in the near-bed layer, in other words the flow erosion rate that we require – rate of particles elevation from the bed $V_{lift} = w \cdot c_0$.

Basically, we just re-interpret the numerous laboratory data regarding *uniform* currents with a *steady state* concentration profile (16) obtained before: not only do we take the suspended transport rate q_s from such data but we re-calculate it into the erosion rate $V_{lift} = f(\tau)$. And then we use the erosion rate during 3D simulation of suspended sediments transfer for more complicated currents different from uniform ones. Amoudry (2008) and Wei et al. (2014) use other formulas for calculation V_{lift} directly through the bed-shear stress τ. But in case of a test example with a uniform steady current, inside a hydraulic flume, these do not provide the same suspended load transport values q_s as in case of 'classic' formulas like (12) or similar. Moreover, formulas for direct calculation V_{lift} involve a number of empirical parameters that are hard to define.

The equation for convective-diffusion exchange of suspended sediments is recorded using the same form as in case of (1), (2):

$$\frac{\partial c}{\partial t} + \nabla \bullet \left[\left(\boldsymbol{u} - w \cdot \boldsymbol{I_Z} \right) c \right] = \nabla \bullet \left[\left(\nu + \nu_t \right) \nabla c \right] \ , \qquad (18)$$

where c – dimensionless volumetric concentration of suspended particles, $\boldsymbol{I_Z}$ – singular vector directed upwards. A format of recording this equation in a conservative form with regard to vertical multilayer flow discretization is specified by Audusse et al., 2011 and Prokofev (2018): the format is standard just like in case of (1), (2). The source term for suspended sediments elevated from the bed by the flow, is not included into the right part (18): it is described using the lower boundary condition. That is why the discrete form of (18) recorded for the lower (near-bed) computation layer includes the supplement V_{lift} instead of convective exchange through the lower surface of this computation layer congruent with the bed.

There are also dozens of empirical formulas for evaluation of bedload sediment transport. For example, the famous software *Flow-3D*® (Wei et al., 2014) uses the formula by Meyer-Peter & Müller (1948), and based on this formula the specific sediments transport ($m^2 s^{-1}$) is calculated based on the established bed-shear stress:

$$q_b = \beta_n \left(\theta - \theta_{CR} \right)^{1.5} \sqrt{\varphi_\rho \cdot g \cdot d^3} \ , \ \text{where} \ \ \theta = \tau / \left(\rho \cdot \varphi_\rho \cdot g \cdot d \right) \ . \qquad (19)$$

Where β_n – dimensionless empirical order 8 coefficient, and the Shields's critical parameter θ_{CR} is proposed to be taken being equal to 0.047 as per the original research by Meyer-Peter & Müller, however, in the later research, for example Wei et al. (2014) it is calculated using the formula by (13) Soulsby (13) (1987), like in case of suspended sediments. For comparison, let's also mention Van Rijn's formula (1984) for bedload sediment transport used by Ahmad et al. (2014) and in the model COHERENS (n.d., Chapter 7):

$$q_b = \frac{0.053}{D_*^{0.3}} \left(\frac{\theta - \theta_{CR}}{\theta_{CR}} \right)^{2.1} \sqrt{\varphi_\rho \cdot g \cdot d^3} \ . \qquad (20)$$

As compared to formula (19), it is significantly different both in its dependence on the particles diameter and indicator of the power to which bed-shear stresses are raised: 2.1 vs 1.5.

In the works by Wei et al. (2014), Ahmad et al. (2014), Zhou (2017), dedicated to studying of 3D numerical simulation of local bed scours due to sediments transport, the critical bed-shear stress or the Shields's critical parameter (13) are normally adjusted with regard to local bed slopes. In case when the angle of an underwater slope is close to the limit one (steepest slope angle) and the current velocity is directed 'down grade', θ_{CR} shall be reduced down to 0. In case when the flow direction is reverse, it is vice versa: θ_{CR} shall increased by two times at the limit. Zhou (2017) specifies that such adjustment is highly important for correct simulation of local scours. Figure 1a shows a diagram for angle designations related to inclined slopes and the flow speed vector. Shields's critical parameter is adjusted based on Soulsby's formula (1997) which is also applied by Wei et al. (2014) и Ahmad et al. (2014)

$$\theta'_{CR} = \frac{\theta_{CR}}{T_m}\left(\cos(\psi)\,\sin(\chi) + \sqrt{\cos^2(\chi)T_m^2 - \sin^2(\psi)\,\sin^2(\chi)}\right) . \qquad (21)$$

Where $T_m = \mathrm{tg}(\chi_{\max})$ – steepest slope angle tangent for packed bed sediments under water (steepest slope angle before grains slide by themselves); is normally $\chi_{\max}$ is set within the range of [28º…32º], $0 \le \chi \le \chi_{\max}$. The adjustment multiplier for θ_{CR} in formula (21) never falls outside the range of [0…2]. In case of sediments (bedload and suspended) transport formulas of type (19), this multiplier is directly used for θ_{CR} as per (21). In case of formulas of type (20) containing θ_{CR} in the denominator, it may only be applied to θ_{CR} contained in the numerator. It is convenient to determine the trigonometric functions included into (21) in the course of practical calculations using scalar products:

$$\cos(\psi) = \frac{\langle \boldsymbol{V}, \boldsymbol{G} \rangle}{|\boldsymbol{V}| \cdot |\boldsymbol{G}|}, \quad \sin^2(\psi) = 1 - \cos^2(\psi),$$

$$\cos^2(\chi) = \left(|\boldsymbol{G}|^2 + 1\right)^{-1}, \quad \sin(\chi) = \sqrt{1 - \cos^2(\chi)},$$

where $\boldsymbol{G} = \nabla Z^b$ – gradient vector for bed surface.

As per Zhou (2017), consideration of steep slope slides formed during bed scour in the numerical model is as important as adjustment of θ_{CR} with regard to local bed slopes as per (21). A diagram of the above mentioned process is given in Fig. 1b: for purposes of simplicity the representation is one-dimensional. The digits given in circles 1 and 2 are used to mark a pair of neighboring nodes of the computation mesh – FV centers. The tangent of the bed inclination angle between the two points is determined based on the bed levels Z_1^b and Z_2^b in these points: $T_{12} = \left(Z_2^b - Z_1^b\right)/\Delta x$. In case $|T_{12}| > T_m$, the slope slide process is included which means that bed levels adjustment is performed, considering T_{12}, for the value of

$$\Delta Z_1^b = \begin{bmatrix} (T_{12} - T_m)/2, & T_{12} > 0 \\ (T_{12} + T_m)/2, & T_{12} < 0 \end{bmatrix}, \qquad \Delta Z_2^b = -\Delta Z_1^b .$$

In the software code that implements such a method, these adjustment levels inside each time step are first recorded in *slide*-array in the form of a bed map and then, once the time step is completed (when all computation nodes are processed), *slide* adjustment is added to current

London Journal of Engineering Research

bed levels. In reality, in case of slope slide, sediments from point 3 not shown on Fig. 1b may be transferred to point 2. This may again lead to violation of the condition $|T_{12}| \le T_m$, but in a specific number of time steps its implementation can be ensured anyway. In case the task is not one-dimensional, slopes starting in this point directed to neighboring nodes are compared to the limit ones, including diagonal directions: in case of the FV regular mesh there are 8 such directions. In case of a curvilinear mesh, *slide* adjustment Z_1^b and Z_2^b is a little more complicated: it is required to take into account the ratio between the areas of the neighboring FV (1 and 2) in order to ensure the sediments mass conservation (scheme conservation) in case of slope slide.

After the dimensionless concentration of suspended sediments during another time step is calculated using the exchange equation (18) and the bedload sediment transport is determined, for example, based on (19), changes of bed levels Z^b are calculated using Exner's equation (Ahmad et al., 2014; Zhou, 2017)

$$\frac{\partial Z^b}{\partial t} = \frac{F}{1-p}\left[-\nabla \bullet \left(q_b \frac{\boldsymbol{\tau}}{|\boldsymbol{\tau}|}\right) - V_{lift}^0 + c_0 \cdot w\right], \qquad (22)$$

where p – soil porosity of 0.4 order of magnitude, $F \ge 1$ – boost factor for bed scours, V_{lift}^0 and c_0 – erosion rate for suspended sediments and their dimensionless concentration at the reference level σ_0. The approach that uses reference levels is specified in the description Delft3D-FLOW (2005). What is important is that this reference level has to be the same when defining the rate of elevation of suspended particles from the bed V_{lift} and their sedimentation – the last term (22). For example, in case of a multilayer model this may be an average level for the lower computation layer: earlier we used it to define V_{lift}. In case of single-layer (planimetric, 2D) models we deal with depth averaged concentrations of suspended sediments $c_m = q_s / q$ where $q = h \cdot \overline{V}$ – specific water discharge (Van Rijn, 2012). We can set, for example, $\sigma_0 = 0.05$. In this case V_{lift}^0 is brought to the erosion level, as it was described earlier, by integration (17) of the Rouse's profile (16) and, in the same manner, in case of the profile (16) transfer from c_m to near-bed concentrations of suspended sediments c_0 at the same level is performed $\sigma_0 = 0.05$: $c_0 = r \cdot c_m$, $r > 1$.

It is important to clarify that we only use Rouse's equilibrium concentrations profile (16) in two cases:

- in case of *interpretation* of data obtained during laboratory experiments involving suspended sediments which is allowable as the current is uniform under such conditions and the concentration profile is steady state;
- in case of a single-layer (planimetric, 2D) task when there is no other way to consider the non-uniformity of distribution of suspended sediments over the depth.

In a 3D case (multilayer model) it is clear that the distribution of concentrations of suspended sediments over the flow depth is more complicated: we take this into account when solving the 3D equation (18), and we only use the equilibrium profile (16) for re-calculation q_s into the erosion rate of the flow $V_{lift}^0(\tau)$.

The first term in the right part (22) reflects the contribution into the bed scours of bedload sediment transport directed along the bed-shear stress vector $\boldsymbol{\tau}$. The boost factor F can be used for demanding computation tasks to reduce the time needed for calculation of bed

scours related to sediments transport (Zhou, 2017, p.64). Such scours take place slowly as compared to the time necessary for the hydrodynamic part of the task to adapt to bed transformations. So in case of some tasks, once check calculations are performed one can take, for example, *F=10* and consider this time boost factor when interpreting the obtained results related to bed scours. The excessive value *F* may lead to calculations instability.

The divergence discrete form in the right part (22) is recorded using the central difference scheme. There was no need to use Zhou's (2017) filter for smoothing the oscillations of increments of the bed levels when solving Exner's equation (22). Once bed scours are calculated using the equation (22), the above described *slide* adjustment of the bed levels is performed additionally: consideration of the bed slides that had a slope angle higher than the limit one during the previous time step.

IV. VALIDATION OF A 3D NUMERICAL MODEL

The multilayer open flow model that was taken as a basis had already been tested earlier by comparing the calculation results with analytic solutions and experimental data. In particular, Prokofev (2017, 2018) validated the hydrodynamic pressure calculation module using wave problems where the difference of the pressure distribution over the flow depth from the hydrostatic one plays a key role. Let's focus only on additional validation of the new software modules described herein: calculation of turbulence parameters and sediments transport simulation.

4.1 Case 1. Turbulence model validation

A standard test to check the applicability of the turbulence model (1)-(5) is a task involving flowing around the spur-dyke by the open flow (Wu et al., 2004) or a task involving the formation of a recirculation zone under a flow in a sudden-expanded flume (Fe et al., 2000; Wu et al., 2004). Calculations were performed for both scenarios. For example, we compared the results of the numerical experiment involving flowing around spur-dyke, as in the research conducted by Wu et al. (2004) with the results of the laboratory experiment A1 by Rajaratnam & Nwachukwu (1983). A hydraulic flume with the width of 0.92 m and length of 37 m; a spur-dyke represented by an aluminum plate with the width of 3 mm and length of 0.152 m is installed in the middle of the flume orthogonally in relation to one of the walls. Flow depth – 0.189 m, discharge rate in the flume – 0.0453 m^3 s^{-1}. During the numerical experiment, a specific discharge level for the inflow (left) boundary was set, and the logarithmic depth profile of the normal velocity component $V_x(\sigma)$ was set, the shear components related to this boundary are $V_y = V_z = 0$. In case of the outflow (right) boundary, only the depth of the flow was registered. The bed roughness coefficient in the Manning formula is $n = 0.012$ $m^{-1/3}s$. In order to find the relevant roughness parameter z_0 in (5), (6) for this *n*, we are going to integrate the logarithmic velocity profile as per *z* within the range $[z_0 \ldots h]$ (Ahmad et al., 2014; Zhou, 2017); this profile provides a good description of the current not only in proximity to the bed but also over the whole depth:

$$U(z) = \frac{U_*}{\mathrm{K}} \ln\left(\frac{z}{z_0}\right).$$

If we compare the linear connection $\overline{U(z)} = a \cdot U_*$ that we obtained with Manning's formula for bed roughness, we find an exponential dependency of re-calculation $n \to z_0$:

$$z_0 = h / \exp\left(\frac{h^{1/6} \cdot \mathrm{K}}{n\sqrt{g}} + 1 \right) \quad . \tag{23}$$

In case of the specified depth parameter h, the formula (23) provides: $z_0 \approx 0.018$ mm.

The length of the calculation domain is 12 m, out of which 4 m are located to the left of the spur-dyke. In case of discretization based on planimetric coordinates a regular orthogonal mesh with 250×60 nodes was used that has a condensation similar to (9) in the spur-dyke area: along the flow axis, the ratio among the computational mesh steps is $\Delta x_{\max} / \Delta x_{\min} = 5.39$, in case of the flume cross section it is $\Delta y_{\max} / \Delta y_{\min} = 2.28$. In vertical direction, a uniform (without condensation) division into 10 layers was used. Similar tasks can be solved in a single-layer (planimetric) configuration and the 10 layers in our case were taken only for validation of the 3D turbulence model. The length of the recirculation zone that forms behind the spur-dyke depends significantly on the choice of the turbulence model and the boundary conditions related to this model; the boundary conditions (7) were set for the free surface. Based on the experimental results obtained by A1 Rajaratnam & Nwachukwu (1983), the length of the recirculation zone is about 2 m: from the spur-dyke downstream. Based on our calculations, its length was 1.85 m in case of using the standard k-ε turbulence model and 2.30 m when using its RNG-type or the non-equilibrium k-ε model. It is impossible to obtain a stable recirculation zone in calculations without taking the viscosity into account and the simplest single-parameter eddy viscosity models reduce its length significantly. Based on our calculations, the maximum value of eddy viscosity in the flow core after the spur-dyke reaches 0.0018 m^2s^{-1} (standard k-ε model), which is a little lower than the value obtained in the calculations by Wu et al. (2004) by means of the same model in a planimetric task: 0.0022 m^2s^{-1}, but close to the calculations by Wu et al. (2004) for the k-ε-RNG model (0.0017 m^2s^{-1}). The time spent by Nvidia GeForce GTX-1080ti GPU to solve this task with the 2.5D configuration does not exceed 5 minutes.

4.2 Case 2. Suspended transport model validation

It is difficult to find any published experimental data where the leading role would be played by suspended sediment transport: normally experiments involve large grain sand when scour deformations are defined primarily by the bedload sediments moving. Nevertheless it is desirable that the method for calculation of suspended sediment concentrations provided herein be also tested at least based on a virtual task. We can at the same time make sure that the software implementation of the k-ε turbulence model described ensures correct vertical distribution of eddy viscosity $\nu_t(\sigma)$: the previous *test 1* could be considered with a planimetric 2D configuration as well, so it only confirms the correctness of distribution simulation $\nu_t(x, y)$. Let's consider uniform steady current in a provisional hydraulic flume with the length of 150 m, flow depth of 3 m and depth-averaged current velocity of 1.5 m s^{-1}. If the bed roughness coefficient based on Manning's formula is $n = 0.016$ $m^{-1/3}s$, the roughness parameter as per (23) is $z_0 \approx 0.06$ mm. The bed-shear velocity at the specified parameters is $U_* \approx 0.062$ m s^{-1}. Let's assume that the flume smooth bottom is covered with even-grained sand $d = 0.1$ mm, $\rho_s = 2650$ kg m^{-3}. At the water temperature of T = 12ºC as

per (11) – $\nu = 1.2 \times 10^{-6}\,\mathrm{m^2 s^{-1}}$, while the grain fall velocity (10) of such sand is $w = 6.65 \times 10^{-3}\,\mathrm{m\ s^{-1}}$. The Rouse's parameter is $w/(U_* \mathrm{K}) \approx 0.27 < 1$, so one can expect that bed particles will transfer into a suspended state. Let's assume that a steady profile over the depth (16) of the sediment particles volumetric concentrations was set for the inlet flume cross section.

We are going to use the numerical scheme provided above involving the *k*-ε turbulence model and the empirical formula (12) to calculate the concentration profile in the outlet section: as the current is uniform, it is expected to represent the same Rouse's equilibrium profile as in case of the inlet to the hydraulic flume. During this test, calculations were performed with regard to the vertical longitudinal cross section of the flume only and the flume was uniformly divided into 15 layers depthwise: in fact, this is a 2D task. Calculation results are summarized in Fig. 2. Rouse's reference profile (16) is shown for which the constant c_0 corresponds to the suspended load transport q_s calculated using Van Rijn's empirical formula. Moreover, Fig. 2 shows the concentration profiles at the outlet of a virtual hydraulic flume obtained using a 15 layer numerical model. The first one was obtained based on soft boundary conditions (7) on the free surface which provides the distribution $\nu_t(\sigma)$ in proximity to it that is different from (14). As is shown in Fig. 2, this leads to deviations of the calculated concentration profile from Rouse's profile based on (14) and this only refers to the area near the free surface: $\sigma > 0.8$. The second concentration profile was obtained with the conditions (7) for *k* and (4) for ε on the free surface – such a possibility was discussed above, which provided vertical distribution of eddy viscosity (14). The second profile is almost identical to the Rouse's reference profile: the insignificant difference that is present is related to the choice of quite a rough (uniform) mesh in the vertical direction. All nodes of this mesh are marked with squares in Fig. 2. Moreover, the *k*-ε turbulence model is not even supposed to provide any perfect match of $\nu_t(\sigma)$ with the single-parameter Montgomery's formula (14) which also leads to insignificant differences among particle concentration profiles in Fig. 2. If we refuse to use the *k*-ε turbulence model and only use the equilibrium profile $\nu_t(\sigma)$ (14), the sediment concentration profile at the outlet boundary will be equal to the Rouse's reference profile (16). This proves that the diffusion components of the exchange equation (18) are approximated with a relatively high level of precision.

In addition to the above, during *test 2* depth-averaged concentrations of suspended particles c_m were compared: the concentration found using the (12) empirical formula and the one found through numerical integration (17) of the calculated concentration profile at the outlet of a provisional hydraulic flume. Their values are: 5.3×10^{-4} and 5.2×10^{-4}, respectively. This good coincidence is not that evident. First of all, each time prior to solving the exchange equation (18), re-calculation of the flow suspended load transport q_s was performed at every next time step with the concentration at the reference level of σ_0, and integration (17) was only performed up to the level $\sigma_{\min}$ – see the description above. Second, the profile $\nu_t(\sigma)$ in proximity to the outlet boundary calculated using the *k*-ε model could be significantly different from the profile (14) at the inlet, in case of mistakes in the algorithm, which would inevitably lead to differences among depth-averaged concentrations.

4.3 Case 3. Scour in a flume: GPU utilized 2D calculations

Test 3 gives a schematic description of formation dynamics of a scour hole and the dune behind it located after the rigid bed area (apron) in the tail race of the hydrosystem with bottom spillway. Vertical section of the laboratory bench of Chatterjee et al. (1994) is given in Fig. 3. The results of the experiment #2 pertaining to this research will be used for validation of numerical models of Abdelaziz et al. (2010), Wei et al. (2014), Zhou (2017). During the experiment, the flow depth h = 0.291 m is recorded at the right outlet boundary. The submerged water jet comes out through the narrow slit near the bed with the height of 2 cm and rate of 1.56 m s^{-1}; the area above the inlet gate is represented by a smooth wall. At a distance of 0.66 m from this wall, the bed is rigid and smooth, then it is made of sand with a median grain diameter of $d_{50} = 0.76$ mm, $\rho_s = 2650$ kg m^{-3}. In accordance with Zhou's (2017) numerical experiment, the sand porosity is $p = 0.43$ and the steepest slope angle is $\chi_{\max} = 29^{o}$.

The sand grain fall velocity found as per (10) with $\nu = 1.2 \times 10^{-6}$ $m^2 s^{-1}$ is w=0.098 m s^{-1}, which corresponds to the data given in the table but is slightly lower than the value used by Zhou (2017) and specified by Chatterjee et al. (1994) that is w=0.122 m s^{-1}. This is not crucial for numerical experiments as during such an experiment the movement of sediments is mostly forced and the calculation formulas for their transport (19) or (20) do not contain the particle fall velocity. Just like in previous *test 2*, here we can use a 2D numerical model for the longitudinal vertical cross section. On the left, the computation domain is limited by the coordinate $x = -0.66$ m that corresponds to the narrow slit with jet outlet. The distribution $V_x(\sigma)$ is set at this boundary and it is uniform within the gate. The right outlet boundary was selected at the point $x = +1.34$ m where the flow comes out freely, and only the water surface level is registered in the numerical model. The end of the rigid bed area is shown by $x = 0$ – Fig. 3. The mesh pitch along the longitudinal coordinate is $\Delta x = 4$ mm, so in total there are 500 finite volumes (FV) with regard to x. 40 computation layers with condensation near the bed were used for the vertical coordinate: when the parameter E=6 is set in (9), the mesh node that is the closest to the bed is located at about 1.5 mm from the bed and the thickness of the near-bed computation layer is about 3 mm (these values may change during transformation of the movable bed). For comparison: Zhou (2017) managed to achieve a remarkable consistency between the numerical simulation results and the experimental data using a more detailed computational mesh with the pitch of $\Delta x = 3$ mm across the longitudinal coordinate and $\Delta z = 2$ mm in vertical direction using a uniform division into 145 layers. Regarding bed transformation equation (22), we set F = 1, so boost was not used in *test 3*. In order to describe the bedload transport in *test 3* and the next *test 4*, empirical formula (19) with the parameter $\beta_n = 4.5$ was used. This value is lower than the value recommended by Wei et al. (2014) and Meyer-Peter & Müller (1948), which is equal to $\beta_n = 8$, but ensures better correspondence to the experiment. The roughness parameter for a rigid smooth bed area is $z_0 = 0.003$ mm, while in case of a sand bed based on the recommendations given by Wei et al. (2014) and Zhou (2017) the value $k_s = 2.5 \cdot d_{50}$, $z_0 = k_s / 30 = 0.063$ mm was used. This is important as z_0 is directly used when calculating bed-shear stresses (6) and these stresses are included into the bedload transport formula raised to the power of 1.5 (19) or even 2.1 (20). When working with formulas of types (19) or (20) that are based on the local value of bed-shear stress one cannot choose the

bed friction parameter z_0 separately from the sand grain median diameter (Zhou, 2017, p.55) for example by means of connecting it with a randomly chosen friction coefficient *n* using formula (23). In more complicated cases when the bed contains large uneven areas (riffles, ridges) friction parameters are set separately (COHERENS, n.d., p.312): 'global' k_b – for the hydrodynamic part of the task and k_s – for sediment transport calculation; k_s is lower; in publications by Van Rijn (2012), Zhou (2017) and the description of COHERENS it is designated using the term '*skin friction*'.

In calculations for *test 3*, the *k*-ε-RNG turbulence model (1)-(3) was used with the soft boundary conditions (7) on the free surface. The longitudinal profiles of the movable areas of the bed for 1, 3, 5, 8, 12, 20 and 30 minute time points obtained based on the calculation results are given in Fig. 4. The agreement with the bed levels recorded during the experiment that are marked with squares on the same figure is quite satisfactory. The dune slope located downstream has an angle that is close to the limit one equal to 29º. Using the *k*-ε turbulence model validated in *tests 1 and 2* during numerical simulation within the context of this experiment plays a key role: simulation of jet current without it, based on single-parameter models used for eddy viscosity ν_t calculation, *failed*. In case of *test 3*, taking into account the non-hydrostatic amendments to the pressure value (Prokofev, 2018) is also mandatory. The adjustment (21) approximates the computation data to the experimental ones significantly: if it is not used, their agreement is much worse that in Fig. 4. The influence of suspended sediments on the calculation results in *test 3* is extremely low.

The full computation time within *test 3* for the above mentioned GPU Nvidia does not exceed 3.5 hours[1] or 10 hours when using a *laptop* with the AMD[2] Radeon R9 M275x graphics processing unit. Analogous calculations performed by Zhou (2017, p.83) using the *OpenFOAM*® open code took 160 hours when using an 8-core CPU even with the algorithm multisequencing and boost activation $F = 5$ in (22). Prokofev (2017, 2018) already specified high efficiency of GPU utilization in algorithms based on an explicit scheme with a random order of computation node processing at each time step.

Let's analyze the numerical simulation results provided by other authors for *test 3*. Zhou (2017, p. 90) provides diagrams similar to Fig. 4 and they demonstrate almost full agreement with the experimental data obtained by Chatterjee et al. (1994). However, it remains unclear why in case of 1 minute time step the lower dune slope has an angle that is larger than the limit one equal to 29º. In case of a physical experiment, this may be explained by both a measurement error and incompleteness of the slope slide process. But how could such an 'extreme' slope be obtained using a numerical model where the slope slide is considered instantaneous (Zhou, 2017, p.60 & Appendix B)?

Abdelaziz et al. (2010) and Wei et al. (2014) when simulating *test 3* used adaptation of the well-known commercial software *Flow-3D*® designed by *Flow Science*: a sediment transport module is integrated into it. Abdelaziz et al. (2010) only managed to obtain agreement between the scour depth and the dune's crest with the experiment values related to initial time steps of 1…8 minutes (full experiment time is 60 minutes). The calculated bed transformation profile itself is far from the value obtained in the experiment, which is directly specified by Abdelaziz et al. (2010) in the conclusions.

Finally, Wei et al. (2014) also specify their results for numerical simulation for *test 3*. Unfortunately, the figures containing consecutive changes of the bed profile obtained from

[1] The time is specified for calculations involving not 1 but 3 vertical cross sections: the minimum quantity allowed by our software.

[2] OpenCL language is used which works over Nvidia, AMD, INTEL processing units.

Flow-3D® are nor superimposed over the experimental curves contained therein. There is visual similarity and the steepest slope angle is well observed. At the same time, analysis of the figures provided by Wei et al. (2014, Fig.8) shows that during the first minute the simulated dune's crest shifts from the rigid bed area by $x_c = 39$ cm (see scheme in Fig. 3) instead of 24 cm as in the physical experiment, and within 3 minutes the dune's crest shifts from the apron by $x_c = 42$ cm instead of the 30 cm calculated during the same experiment.

Then the dune movement in the numerical simulation by Wei et al. (2014) gets slower and after 30 minutes it almost stops: 2-cm displacement during the next 30 minutes instead of 8 cm as shown in the measurements. In other words, no reliable consistency between the results obtained by Wei et al. (2014) and the experimental data related to the dune movement *dynamics* is observed, though, just like in our research, the same bedload transport formula (19)[3] and the same adjustment θ_{CR} (21) were used and the slide of steep slopes was taken into account; it was not considered by Abdelaziz et al. (2010).

The analysis that was performed shows that *test 3* is quite complicated for validation of computation algorithms and the software packages.

4.4 Case 4. Scour around big vertical cylinders: GPU based 3D simulation

With the purpose of approbation of sediment transport numerical models and movable bed transformations, simulation of bed scours in a hydraulic flume in proximity to the circular cylinder (pile) is widely used. In most cases, the data obtained in small-scale physical experiments are used for comparison when the cylinder diameter does not exceed 0.2 m (Ahmad et al., 2014; Kim et al., 2017; Zhou, 2017). In proximity to the pile, a complex condition of eddy currents is observed: downstream currents and whirlwinds with a horizontal axis predominate near its front, while behind the pile, there are unstable eddy currents with a vertical axis (Zhou, 2017). In case of such a task, numerical simulation can be performed only with a 3D configuration, it is mandatory to take into account the difference between the vertical distribution of hydrodynamic pressure and the hydrostatic pressure and use the turbulence model for the hydrodynamic model closure. These calculations require significant computation efforts, f.e. Zhou (2017, p.142) spent 1,160 hours (1.5 months) to perform erosion simulation in proximity to the cylinder with the diameter of 0.1 m using the *OpenFOAM*® open code and an 8-core CPU. This simulation covered only the first 30 minutes of the 3 hours of the whole physical experiment duration.

The most interesting experimental data related to transformation of sand bed in proximity to circular cylinders with various diameters as influenced by stationary currents in a hydraulic fume are given in the report by Sheppard (2003). The research was performed at the University of Florida (USA) and completed in 2003. The experiments were performed in a hydraulic flume with the width of 6.1 m, depth of 6.4 m and length of 38.4 m, with 9.8 m occupied by the movable area. Sand bed erosion with a median grain diameter of d_{50}= 0.22 mm, 0.8 mm and 2.9 mm was studied in proximity to circular cylinders with the diameter of 0.114 m, 0.305 m and 0.915 m, and various combinations were analyzed. Flow depth and speed varied: in total, 14 tests were performed and the duration of some of these tests amounted to 579 hours (experiment #14). All the necessary flow physical parameters, including the water temperature, were registered – ref. to (11); by means of an acoustic transponder and two miniature video cameras, the development of scour deformations in time was observed. The flow speed was defined based on two electromagnetic flow meters:

[3] Wei et al. (2014) applied formula (19) with $\beta_n = 8.0$ (default value).

western/eastern, and the discharge was measured based on the measurement weir. The time dependences of the maximum scour depth value are given in the report by Sheppard (2003) in the form of tables and graphics.

In order perform validation of the numerical model, we chose four tests from the report by Sheppard (2003), involving circular cylinders with the biggest diameter of 0.915 m: these are experiments #3, #4, #7 and #14. For all the relevant numerical tests, the following was used:

- The *k*-ε-RNG turbulence model with the boundary conditions (7) on the free surface;
- in case of the inlet boundary – logarithmic distribution of longitudinal velocities $V_x(\sigma)$, tangential velocity components $V_y = V_z = 0$;
- in case of the outlet boundary, only the water surface level was fixed;
- the lateral walls of the hydraulic flume and cylinder surface are smooth (which means that additional TKE production rate is absent) and impermeable;
- Van Rijn's formula (12) for description of the movement of suspended sediments[4];
- Meyer-Peter & Müller formula (18) for bedload sediment transport with the parameter $\beta_n = 4.5$ – like in previous *test 3*: as it was already specified in the introduction, we are not trying to adjust the numerical model to each particular experiment but carry out its *calibration only once;*
- sand bed roughness parameter $z_0 = k_s / 30$, where $k_s = 2.5 \cdot d_{50}$: the same as in *test 3*;
- porosity for quartz sand $p = 0.4$, steepest slope angle $\chi_{\max} = 30^{\circ}$;
- boost factor *F* in (22): during the first 2.5 minutes, the current stabilizes and the bed erosion is not active, *F*=0; during the next 2.5 minutes, bed scours boost is activated with *F*=10; then, during 25 hours *F*=60 is applied (1 minute of hydrodynamic computation corresponds to 1 hour of morphometrical computation), and then – *F*=180; during the final bed scour stage even *F*=360 may be set which does not cause algorithm instability or affect the results;
- uniform orthogonal mesh along the planimetric coordinates 541×254 of nodes for the computational domain $x \in [-6, +7]\,\text{m}$, $y \in [-3.05, +3.05]\,\text{m}$; condensation of the horizontal mesh in proximity to the cylinder that has its center in *x=y=0* was not applied: the UNO flux reconstruction scheme described above ensures sufficient accuracy of approximations; computational mesh pitch $\Delta x = \Delta y = 0.024$ m;
- condensation parameter near the bed of the vertical computational mesh in (9) *E* = 6.

Now let us list the parameters that differ in experiments #3, #4, #7 and #14.

Experiment #3: median grain diameter of the bed material $d_{50} = 0.8$ mm, average flow depth $h = 1.27$ m, water temperature[5] $T = 8.5\,^{\circ}\text{C}$, depth averaged flow speed $\overline{V} = 0.4\ \text{m s}^{-1}$ – was taken as an average value between the western and the eastern velocity sensor); experiment duration $t_{\max} = 362$ hours; in vertical direction we used $L = 36$ computation layers.

[4] In case of the experiments selected, suspended sediments do not play any significant role.

[5] The experiments themselves were performed at the USGS Laboratory, Massachusetts, not in Florida.

London Journal of Engineering Research

Experiment #4: $d_{50} = 0.8$ mm, $h = 0.87$ m, $T = 0.5$ °C, $\overline{V} = 0.365$ m s^{-1}, $t_{\max} = 164$ hours: the report by Sheppard (2003) specifies the time equal to $t_{\max} = 143$ hours, but data for 21 more hours are also given; L=25.

Experiment #7: $d_{50} = 2.9$ mm, $h = 1.22$ m, $T = 0.7$ °C, $\overline{V} = 0.755$ m s^{-1}, $t_{\max} = 188$ hours; $L = 36$.

Experiment #14: $d_{50} = 0.22$ mm, $h = 1.81$ m, $T = 23$ °C, $\overline{V} = 0.3$ m s^{-1}, $t_{\max} = 579$ hours; $L = 45$.

The computation time when using the Nvidia GeForce GTX-1080ti game graphics processor unit in case of #3, #4 and #7 experiments amounted to 82, 23.5 and 53 hours respectively. This is a relatively short time period for such large scale 3D tasks, and the major part of this time period is spent on solving the Poisson's equation for non-hydrostatic pressure correction by using the simplest iteration method (Prokofev, 2018). As even when the boost factor F in (22) is considered, the bed transformation rate is extremely slow, the task is close to a stationary one and the iterations converge very fast. For purpose of achieving the *correction* of the pressure 10^{-6} (the correction *convergence* is compared to the hydrostatic pressure at the same depth), 12 iterations are more than adequate for each time step.

Calculations related to experiment #14 take longer time: its duration at the laboratory is longer and when performing calculations more layers in vertical direction are required as the flow deeper. It seems that high computation efforts are the reason why we have not found any publications where any experiment described in the report by Sheppard (2003) would be reproduced using a numerical model. Nevertheless, application of GPU (Prokofyev, 2017) allows to simulate experiment #14 as well within 7 days of computation, which is quite acceptable. In this case, only 14% (1.5Gb) of GPU RAM were loaded.

The dynamics of the scour hole depth obtained as a result of numerical simulation of the maximum depth per the computation domain is given in Fig. 5-6. It also contains symbols corresponding to the experimental data by Sheppard (2003). In general, the agreement may be considered good, and in case of experiment #14 it is almost full. The highest disagreement with the test results is observed at the scour initial phase: it reaches about 10% in case of experiments #3, #4 and #7. The final depth of the scour hole is calculated better: the error is up to 5% in case of experiments #3 and #14, and in case of #4 and #7 it is negligible. The average curve slope, namely the calculated erosion rate agrees well with the experimental data. The scour curve pulsations for experiment #4 in Fig. 5 are related to the movement of riffles on the scour hole bed; a 3D visualization of transformations is referred to in (Prokofev, 2019). For clarity, Fig. 5-6 contains the second curve (lower continuous line): it refers to scour dynamics at a fixed point $x = -0.41$ m, $y = +0.41$ m,, which means approximately in the score hole focus – near the cylinder front at the angle of 45º from the axis of the hydraulic flume. There, these bed scour pulsations manifest themselves more, as compared to the upper curve of the maximum scours.

It is interesting that in case of experiment #14 the sand is 13 times finer as compared to #7: the range of grain diameters is quite wide. Nevertheless, we managed to achieve good agreement between the calculation results and the data gathered in each of the four experiments, without changing the empirical parameters selected during the primary (*single*) calibration during *test 3*.

The choice of the boundary conditions type for the k, ε turbulence parameters on the free surface has little influence on the results of *tests 3 and 4*. The role of suspended sediments (considered by us) is insignificant, in the course of numerical research by Ahmad et

al. (2014) in respect of bed scours near the cylinder $D = 0.2$ m with sand $d_{50} = 0.92$ mm, suspended sediments were not taken into account at all.

V. CONCLUSIONS

The use of even the simplest empirical formulas for sediment transport in 3D numerical models in combination with the modern computation technologies (OpenCL, CUDA) allows to simulate complicated scours of a movable bed within a reasonable time period ensuring sufficient accuracy.

The algorithm described herein can find practical use in forecasting of local scours in proximity to bridge supports, breakwater pier heads, in a hydrosystem's tail races after the bottom spillways, and other tasks where three-dimensional current effects play a significant role. Further direction for research is validation of the algorithm based on the experimental data where the movable bed transformations are also provided by waves (Ahmad et al., 2014). The method included into the software package already allows to perform such calculations (Prokofev, 2017, 2018).

VI. SUPPLEMENTAL DATA

Supporting materials for test calculations of Case 1 involving flowing around the spur-dyke and a test involving the formation of a recirculation zone in case of a flow in the sudden-expanded flume can be accessed from Prokofev (2019). Additional graphical materials, including current plans and bed scour process animation, given in the test Case 4 are available at the same source. Moreover, the text files available referred to in Prokofev (2019) contain the saved data of laboratory experiments for validation of Case 3 and Case 4.

Notation

c = suspended sediment's volumetric concentration (-)
c_m = depth averaged suspended sediment's concentration (-)
c_0 = volumetric concentration at reference level σ_0 (-)
$C_\mu, C_{1\varepsilon}, C_{2\varepsilon}$ = turbulence's model constants (-)
FV = finite volume (mesh cell)
d = sand particle size (m)
d_{50} = median grain size (m)
D_* = dimensionless sand particle size (-)
E = vertical σ- mesh thickening factor (-)
F = bed transformation boost parameter (-)
g = gravity acceleration (m s^{-2})
$\boldsymbol{G}$ = bed slope gradient vector (-)
h = flow depth (m)
k = turbulence kinetic energy, TKE (m^2s^{-2})
k_s = Nikuradse's roughness height (m)
K = Von Karman's constant = 0.41 (-)
L = vertical σ- mesh layers amount (-)
M_e = sediment's mobility parameter (-)
n = Manning formula's friction coefficient ($m^{-1/3}s$)

q_b = bedload sediment transport rate (m^2s^{-1})
q_s = suspended load sediment transport rate (m^2s^{-1})
p = packed sand bed porocity (-)
$Prod$ = TKE generation source term (m^2s^{-3})
t = time (s)
T = water temperatute (ºC)
T_m = tangent of the steepest slope angle (-)
$\boldsymbol{u}$ = liquid current velocity vector $[u_1, u_2, u_3]$ (m s^{-1})
U_* = bed shear velocity (m s^{-1})
$\boldsymbol{V}$ = current velocity vector in a near-bed calculation layer (m s^{-1})
$\overline{V}$ = depth averaged current velocity (m s^{-1})
$V(\sigma)$ = vertical profile of the longitudional current velocity (m s^{-1})
V_{CR} = depth averaged critical velocity (m s^{-1})
V_{lift} = lifting velocity for a suspended particles: erosion rate (m s^{-1})
V_{lift}^0 = lifting velocity at the reference level σ_0 (m s^{-1})
w = sand particle fall velocity (m s^{-1})
x, y, z = coordinates (m)
z^+ = distance from the bed to the nearest mesh node (m)
z_0 = bed roughness parameter (m)
β_n = calibration factor for bedload transport formula (-)
$\Delta x, \Delta y$ = mesh cell (FV) sizes for x and y directions (m)
ε = TKE dissipation rate (m^2s^{-3})
θ_{CR} = critical Shields parameter (-)
ν = water kinematic viscosity (m^2s^{-1})
ν_t = eddy viscosity (m^2s^{-1})
ρ = water density (kg m^{-3})
ρ_s = sediment grains density (kg m^{-3})
σ = dimensionless vertical coordinate [0…1] (-)
σ_0 = dimensionless reference level (-)
σ_k, σ_ε = turbulence's model constants (-)
τ = bed shear stress (N m^{-2})
φ_ρ = relative density (-)
χ_{max} = steepest slope angle before grains slide by themselves (deg)

REFERENCES

1. Abdelaziz, S., Bui, M.D., Rutschmann, P. (2010). Numerical simulation of scour development due to submerged horizontal jet. *River Flow - Dittrich, Koll, Aberle & Geisenhainer (eds), Bundesanstalt für Wasserbau, ISBN 978-3-939230-00-7,* 1597-1604.
2. Ahmad, N., Bihs, H. , Kamath, A., Arntsen, Ø.A. (2014). 3D Numerical modelling of pile scour with free surface profile under waves and current using the level set method in model REEF3D. 8p. Retrieved from http://eprints.hrwallingford.co.uk/1575/1/PA_3_20-Ahamd-N.pdf.

3. Amoudry, L. (2008). A review on coastal sediment transport modelling. *Proudmat Oceanofgaphic laboratory, #189*. Retrieved from http://nora.nerc.ac.uk/id/eprint/8360/1/POL_ID_189.pdf
4. Audusse, E., Bristeau, M-O., Perthame, B., Sainte-Marie, J. (2011). A multilayer Saint- Venant system with mass exchanges for shallow water flows. Derivation and numerical validation. *ESAIM: M2AN, v.45(1),* 169-200. Retrieved from https://arxiv.org/pdf/0901.3887.pdf
5. Belov, I.A., Kudriavtsev, N.A. (1987). *Teplootdacha i soprotivlenie paketov trub [Heat transfer and resistance of pipe packages]*. Leningrad, RUS: Energoatomizdat, 223p.
6. Chatterjee, S.S., Ghosh, S.N., Chatterjee, M. (1994). Local scour due to submerged horizontal jet. *Journal of Hydraulic Engineering, 120(8),* 973-992.
7. COHERENS. (n.d.) Chapter 7. Sediment transport model. *Royal Belgian Institute of natural science*. Retrieved from https://odnature.naturalsciences.be/downloads/coherens/documentation/chapter7.pdf
8. Delft3D-FLOW. (2005). Chapter 11: 3D Sediment transport and morphology. *User manual. Delft hydraulics*. Retrieved from ftp://ftp.coastal.la.gov/Whiskey%20Island/TE-47/Appendix%20A%20-%20D3D%20Sediment%20transport%20and%20morphology.pdf.
9. Fe, J., Navarrina, F., Puertas, J., Vellando, P., Ruiz, D. (2000). Experimental validation of two depth averaged turbulence models. *International Journal for Numerical Methods in Fluids,* 00:1-6, 25p.
10. Kim, H.S., Roh, M., Nabi, M. (2017). Computational modeling of flow and scour around two cylinders in staggered array. *Water, 9(654),* 19p.
11. Kulikovskii, A.G., Pogorelov, N.V., Semenov, A.IU. (2001). *Matematicheskie voprosy chislennogo resheniia giperbolicheskikh system uravnenii [Mathematical problems of numerical solution of the hyperbolic systems of equations]*. Moscow, RUS: Fizmatlit, 608p.
12. Kuzmin, D., Mierka, O., Turek, S. (2007). On the implementation of the κ-ε turbulence model in incompressible flow solvers based on a finite element discretization. *International Journal of Computing Science and Mathematics, vol. 1(2)*. DOI: 10.1504/IJCSM.2007.016531.
13. Lin, P., Liu, P.L.-F. (1998). A numerical study of breaking waves in surf zone. *Journal of Fluid Mechanics, vol.359*. 239-264.
14. Ma, G., Shi, F., Kirby, J.T. (2012). Shock-capturing non-hydrostatic model for fully dispersive surface wave processes. *Ocean Modeling, vol.43-44*. 22-35.
15. Meyer-Peter, E., Müller, R. (1948). Formulas for bed load transport. *Stockholm: Proc. 2nd Meeting International Association of Hydraulic Research*. 39–64.
16. Prokofev, V. (2018). Multilayer open flow model: A simple pressure correction method for wave problems. *International Journal for Numerical Methods in Fluids, vol.86(8)*. 518- 540.
17. Prokofev, V. Supporting materials. (2019) : http://gofile.me/2Zesj/xH3BDPpqv
18. Prokofyev, V.A. (2017). GPU utilization for speed up the solution of the three-dimensional engineering tasks of open flows hydraulics. *Matematicheskoe modelirovanie [Mathematical modeling], vol.29(8)*. 74-94. http://mi.mathnet.ru/eng/mm/v29/i8/p74
19. Rajaratnam, N., Nwachukwu, B.A. (1983). Flow near groin-like structures. *Journal of Hydraulic Engineering, 109(3)*. 463-481.
20. Rodriguez-Cuevas, C., Couder-Castañeda, C., Flores-Mendez, E., Herrera-Díaz, I.E., Cisneros-AlmazanR. (2014). Modelling shallow water wakes using a hybrid turbulence model. *Journal of Applied Mathematics, ID 714031*. 10p.
21. Sheppard, D.M. (2003). Large scale and live bed local pier scour experiments. Phase1: large scale, clear water scour experiments. *Final report. University of Florida*, 199p. Retrieved from https://fdotwww.blob.core.windows.net/sitefinity/docs/default- ource/content/structures/structuresresearchcenter/final- reports/bb473_rpt1.pdf?sfvrsn=d9346f23_0

22. Soulsby, R. (1997). *Dynamics of marine sands*. London: Thomas Telford Publications.
23. Stelling, G., Zijlema, M. (2008). Efficient computation of surf zone waves using the nonlinear shallow water equations with non-hydrostatic pressure. *Coastal Engineering, vol.55*. 780- 790.
24. Török, G.T., Baranya, S., Rüther, N. (2017). 3D CFD modeling of local scouring, bed armoring and sediment deposition. *Water, 9(56)*. 23p.
25. Van Rijn, L.C. (2012). Simple general formulae for sand transport in rivers, estuaries and coastal waters [Monograph]. Retrieved from http://www.leovanrijn-sediment.com/papers/Formulaesandtransport.pdf
26. Violeau, D., Issa, R. (2007). Numerical modelling of complex turbulent free-surface flows with the SPH method: an overview. *International Journal for Numerical Methods in Fluids, vol.53*. 277-304.
27. Voltsinger, N.E., Klevannyi, K.A., Pelinovskii, E.N. (1989). *Dlinnovolnovaia dinamika pribrezhnoi zony [Long-wave dynamics of the coastal zone]*. Leningrad, RUS: Gidrometeoizdat, 273p.
28. WAQUA/TRIWAQ (n.d.) - two- and three-dimensional shallow water flow model. Technical documentation. *SIMONA report #99-01, Rijkswaterstaat*. Retrieved from http://simona.deltares.nl/release/doc/techdoc/waquapublic/sim1999-01.pdf
29. Wei, G., Brethour, J., Grünzner, M., Burnham, J. (2014). Sedimentation scour model. *Flow Science report, #03-14*. Retrieved from. https://www.flow3d.com/wp-content/uploads/2014/06/Sedimentation-Scour-Model.pdf
30. Wu, W., Wang, P., Chiba, N. (2004). Comparison of five depth-averaged 2-D turbulence models for river flows. *Archives of Hydro-Engineering and Environmental Mechanics, vol.51(2)*. 183-200.
31. Zhou, Lu. (2017). Numerical modelling of scour in steady flows. *These de doctorat, Ecole Doctorale #162*. Lyon: L'Universite de Lyon. Retrieved from https://tel.archives-ouvertes.fr/tel-01598600/file/TH_T2567_lzhou.pdf

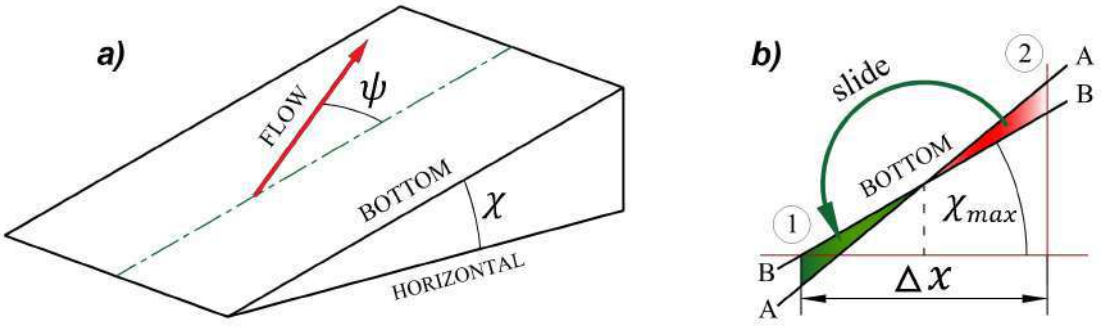

Figure 1: a) diagram of inclined bed for the adjustment of the Shields critical parameter using Soulsby's formula (21); b) the bed slope slide A-A with an angle higher than the steepest slope angle χ_{max} into the stable position B-B; the FV cell face is shown with a dotted line

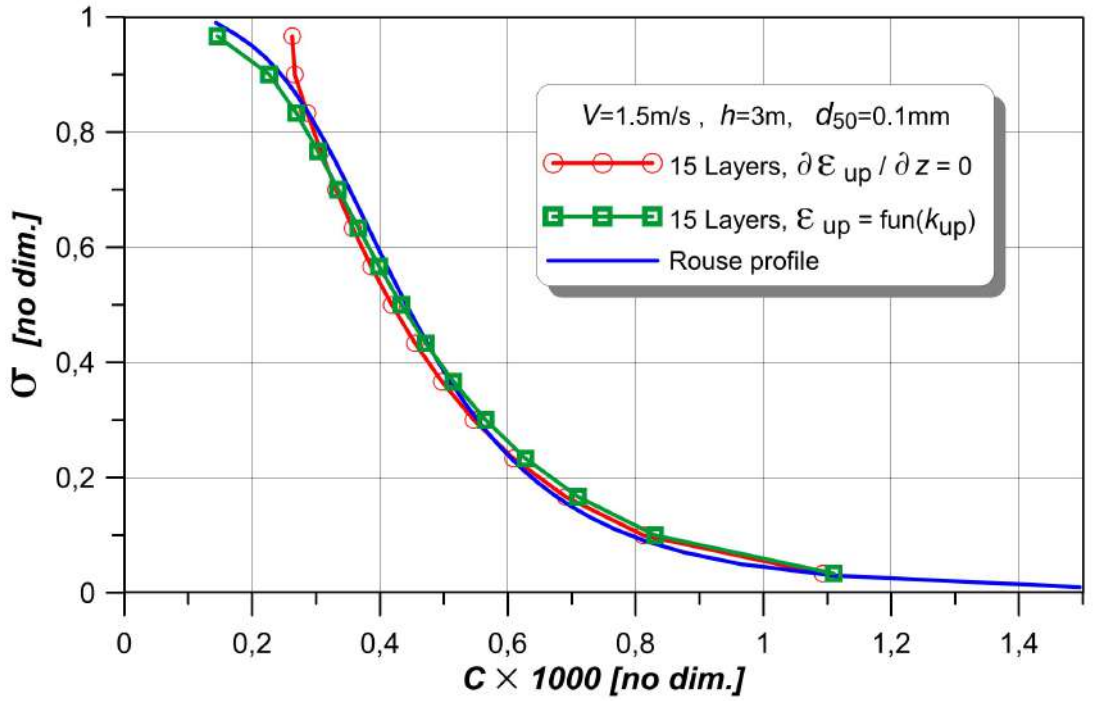

Figure 2: Steady state depth distribution of the suspended particles volumetric concentrations in uniform flow for various calculation schemes

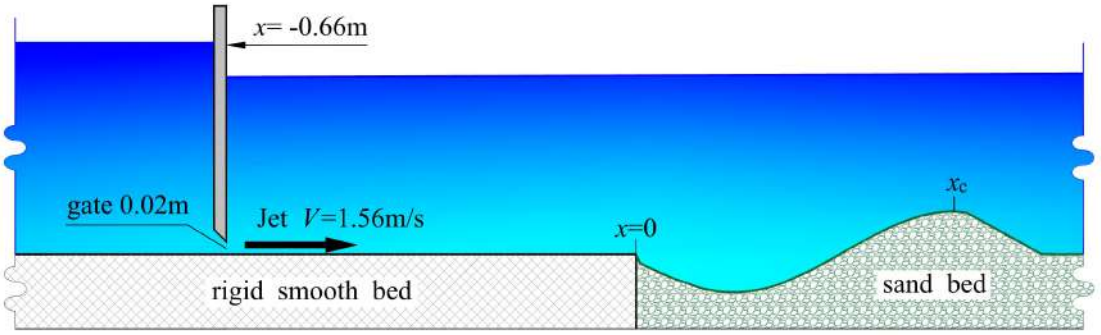

Figure 3: Design of the laboratory experiment by Chatterjee et al. (1994); the scales along x and z are the same; the bed computation profile corresponding to a 30 minute time period is used on the right

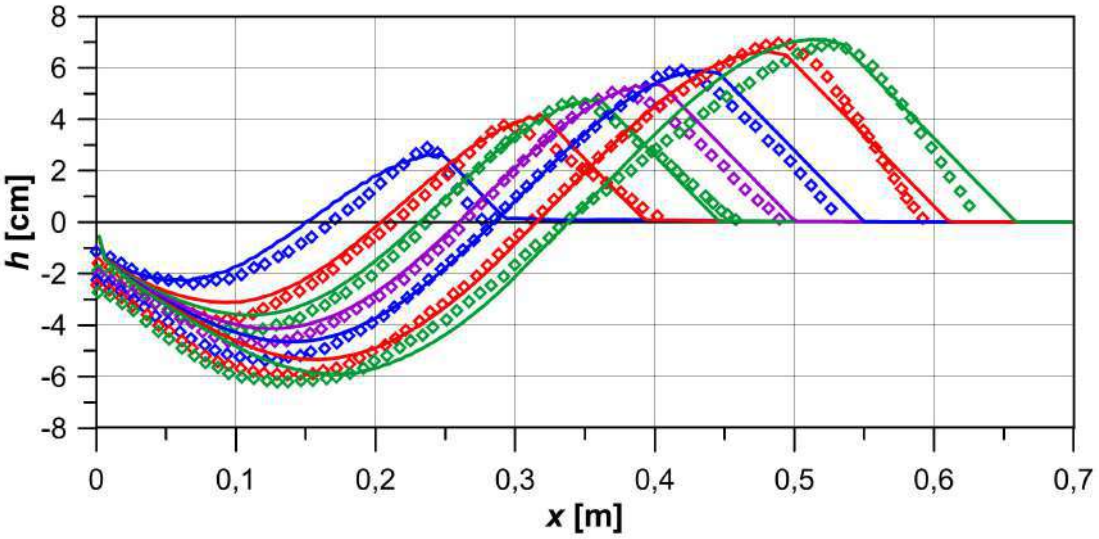

Figure 4: Longitudinal profiles of a movable bed for the time periods of 1, 3, 5, 8, 12, 20 and 30 minutes: obtained in a numerical experiment (continuous lines) and registered in the hydraulic flume by Chatterjee et al. (1994) (squares)

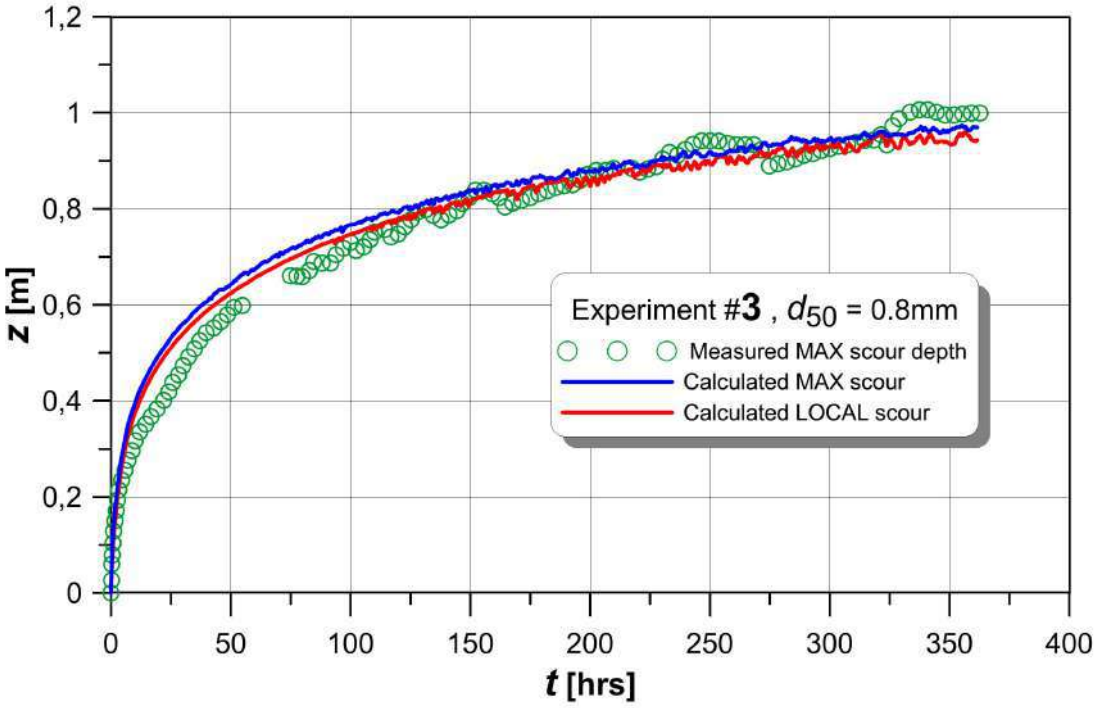

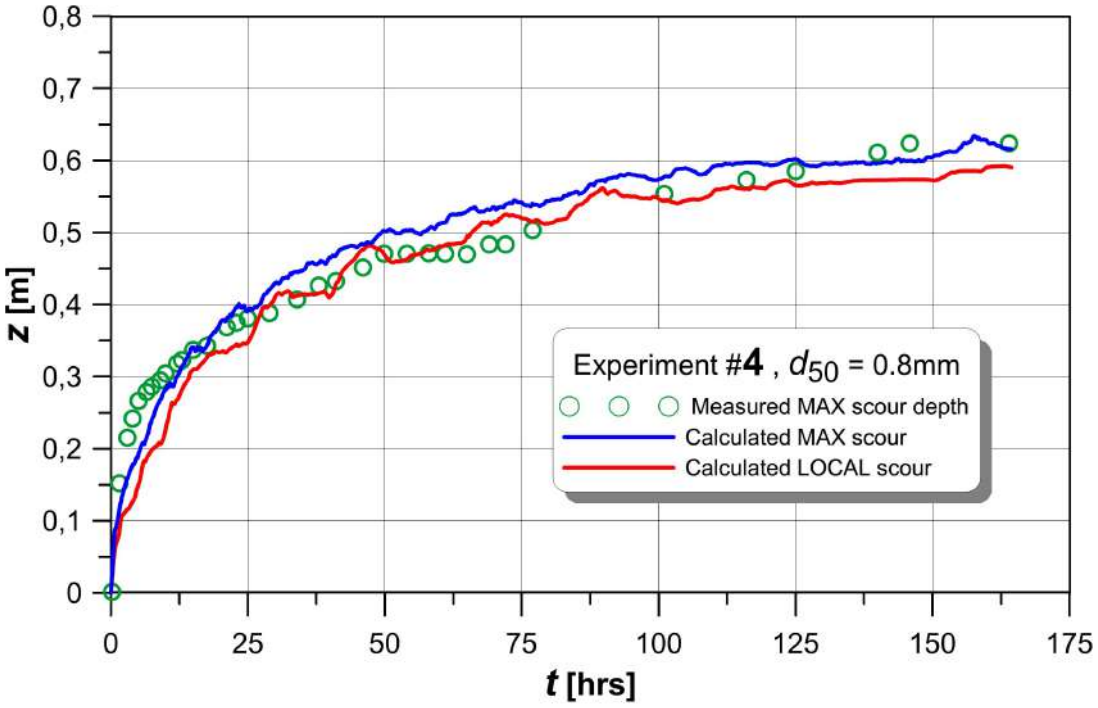

Figure 5: Simulation of bed scour dynamics near the circular pile D = 0.915 m for experiments #3, #4 from Sheppard's (2003) report; upper continuous line – maximum scour depth per the computational domain, lower line – scour depth at the fixed point x = ⁑ 0.41 m, y = +0.41 m

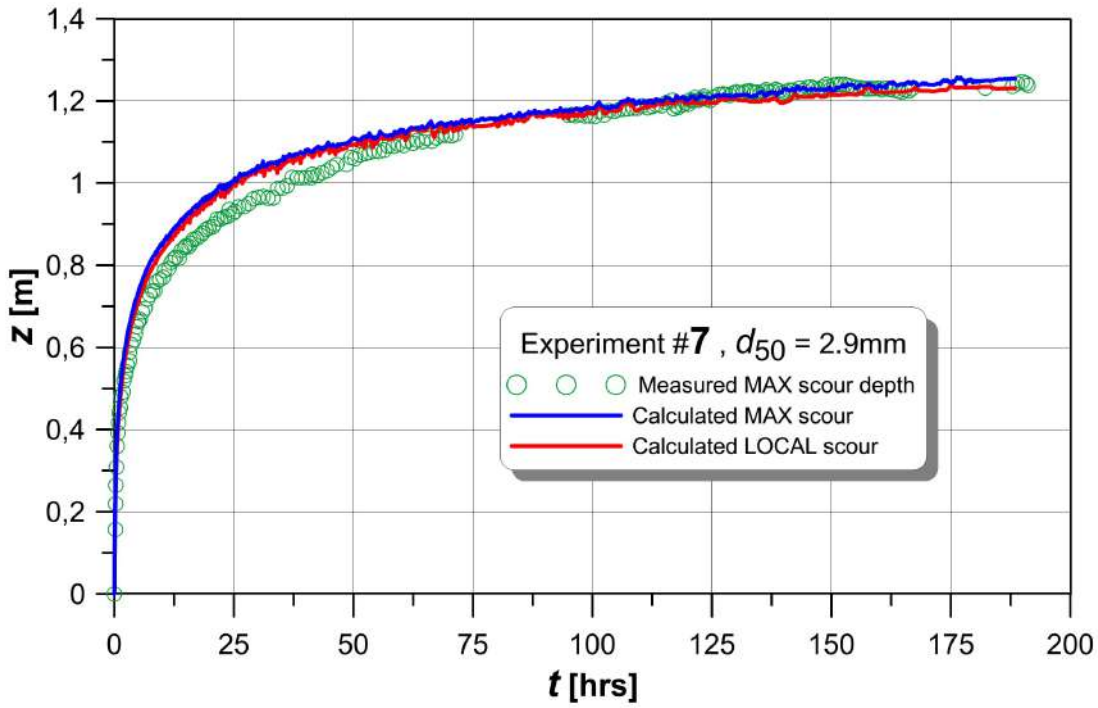

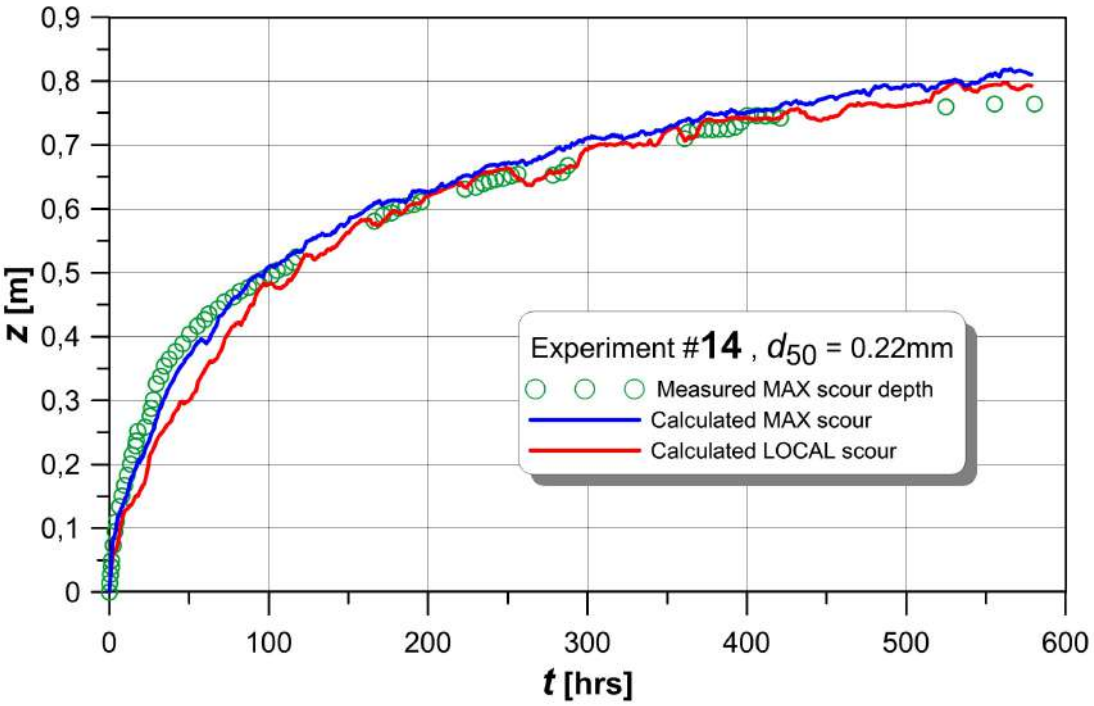

Figure 6: Simulation of bed scour dynamics near the circular pile experiments #7 and #14 from Sheppard's (2003) report D = 0.915 m for